Testing dynamical stabilization of complex Langevin simulations of QCD

Michael Westh Hansen* and Dénes Sexty
Institute of Physics, NAWI Graz, University of Graz, Universitätsplatz 5, Graz, Austria

(Received 11 June 2024; accepted 25 February 2025; published 14 March 2025)

We study complex Langevin simulations of a toy model as well as QCD, supplemented with a dynamical stabilization (DS) term, which was proposed to regularize the complexified process at lower temperatures. We compare the results to reweighting from zero chemical potential to measure the bias that the inclusion of the stabilization term causes, depending on its strength. At high temperatures the stabilization term is not needed. At low temperatures (below deconfinement transition) the DS term has a beneficial stabilizing effect, but too strong a DS term causes phase quenching on the system. We observed that the bias of the dynamical stabilization can, with good accuracy, be removed by extrapolating to zero dynamical stabilization force using a sigmoid fit.

DOI: 10.1103/PhysRevD.111.054508

I. INTRODUCTION

Investigations of the phase diagram of quantum chromodynamics (QCD), needed, e.g., to understand high density states of nuclear matter in neutron stars are hindered by the sign problem. The sign problem is introduced by the fermionic degrees of freedom, which contribute a complex determinant in the measure at nonzero chemical potential μ.

There have been many methods proposed to circumvent the sign problem of lattice QCD (and other theories). The reweighting technique shifts the sign problem into the observable by choosing to simulate in a positive ensemble [1–3]. The Taylor expansion uses simulations at $\mu = 0$ to measure derivatives of the partition function (which are charge densities and charge fluctuations) to extrapolate to finite μ [4–7]. In the analytical continuation method, one uses imaginary chemical potentials for simulations, as the theory is again positive there, and in effect extrapolates results from $\mu^2 \leq 0$ to $\mu^2 > 0$ [8–11].

The general behavior of the above mentioned extrapolation methods is that as long as we are interested in small chemical potentials, they give consistent and reliable results, and their range of applicability depends on the temperature T. Around $\mu/T \simeq 1$ (corresponding to $\mu_B/T \simeq 3$ with the baryon chemical potential μ_B), results start to deteriorate, the different methods give inconsistent results. Further methods used with varying amount of success are the density of states methods [12,13], canonical ensembles [14,15], and dual formulations [16]. For more details and further references, see the reviews [17,18].

The next group of methods exploits the complex analytical properties of the theory: the complex Langevin method, the Lefschetz thimble, and related methods. The complex Langevin method [19,20] is a straightforward generalization of the real-Langevin method (also known as "stochastic quantization") for complex actions, and it does not rely on the interpretation of the measure e^{-S} as a probability, therefore it circumvents the sign problem. The complex action in turn leads to the complexification of the field manifold, and thus a stochastic process on this enlarged space, for which an analytic continuation is used to recover the original theory. One drawback of the complex Langevin method is that in some cases it gives incorrect results. The theoretical understanding of the failure modes have improved significantly [21–27] and diagnostic tools such as boundary terms [28–30] were introduced as well as other diagnostic observables [31,32]. Recently it was shown that the wrong convergence in some cases can be alleviated using the kernel freedom of the complex Langevin method [33–36], which itself uses modern machine learning inspired techniques.

In naive complex Langevin simulations of gauge theories one observes an uncontrollable growth of fluctuations as the fields explore the noncompact complexified manifold of the gauge degrees of freedom. This is negated by gauge cooling [37–41], which uses the gauge degree of freedom to keep the fields close to the real manifold. This in turn makes simulations of gauge theories using the complex Langevin equation (CLE) possible, and it was used to map the whole phase diagram of heavy-dense QCD (which is an approximation for QCD for heavy quarks at large chemical potentials) [42]. It was shown that with gauge cooling one can simulate full QCD at high chemical potentials [43–50]. At high temperatures the equation of state was

*Contact author: michael.hansen@uni-graz.at

also measured at large chemical potentials [51,52], although not yet at physical quark masses.

Dynamical stabilization was proposed to help complex Langevin simulations [53] (see also [54]), keeping their fluctuations in imaginary directions small. It is an *ad hoc* addition to the drift terms of the theory, which present a force pushing the fields towards the real manifold. It can also be viewed as a soft cutoff in imaginary directions which limits the deviation of the fields from the real manifold. It was used in context of the heavy dense QCD as well as for full QCD [52]. In this paper we study the effects of dynamical stabilization on a toy model and in QCD simulations. We quantify its effect on the results of the CLE simulations as a function of the strength of the stabilization force and demonstrate that its functional dependence is well described with by a sigmoid fit and thus extrapolation to zero dynamical stabilization allows us to remove most of the effects of the stabilization on the results.

In Sec. II we give a short introduction to the complex Langevin method and the boundary terms as well as the dynamical stabilization, and describe the systems we investigate. In Sec. III we describe our numerical results, and finally in Sec. IV we conclude.

II. COMPLEX LANGEVIN EQUATION AND NUMERICAL SETUP

In this paper we investigate models with nonzero chemical potential, which means the action S as well as the measure e^{-S} is in general complex. This invalidates naive importance sampling simulations, such as the Metropolis-Hastings algorithm. This problem is known as the sign problem, as the accept/reject step is rendered undefined due to negative- (and in general complex-) valued probabilities.

It is possible to go around the sign problem in some cases using the reweighting method, which pushes the nonpositive part of the measure into the observable. This works well if the sign problem is mild (the chemical potential is small enough). For a severe sign problem reweighting becomes unusable due to a signal-to-noise ratio problem. Due to the overlap problem observables will be dominated by very few configurations, which means that the distribution of the observables is far from a Gaussian and thus naively calculated error bars are also untrustworthy.

For larger values of the chemical potential one has to investigate different methods, and here we will look into the complex Langevin approach. This is based on stochastic quantization, which we briefly introduce below. In this approach we form a stochastic process, which equilibrates to the measure we are interested in, namely $\rho(x) \propto e^{-S(x)}$ for some real action $S(x)$. This can be achieved using the stochastic differential equation called a Langevin equation, which is set up for the variables of our action. Written for a single degree of freedom it is given by

$$dx(\tau) = K(x)d\tau + dw_\tau, \tag{1}$$

where τ is the Langevin time [similar to Monte Carlo (MC) time in usual importance sampling simulations], the drift term $K[x]$ is calculated from the action $K[x] = -\partial_x S$, and dw_τ is the increment of a Wiener process with variance $\langle dw(t)^2 \rangle = 2dt$. This stochastic process implies the Fokker-Planck equation for the probability density $P(x,\tau)$:

$$\frac{\partial}{\partial t}P(x,\tau) = \frac{\partial}{\partial x}\left[\left(\frac{\partial}{\partial x} - K(x)\right)P(x,\tau)\right]. \tag{2}$$

It is easy to see that the stationary measure $P(x) = e^{-S(x)}$ satisfies this equation, and one can show that except for certain special cases this is a unique stationary state and the process equilibrates to it for real actions [55]. On the right-hand side of the Fokker-Planck equation the operator acting on $P(x,\tau)$ is also known as the Langevin operator.

Thus the Langevin equation then forms our stochastic process, which can be discretized using, e.g., the Euler-Maruyama scheme,

$$x(\tau+\epsilon) = x(\tau) + \epsilon K[x(\tau)] + \sqrt{\epsilon}\eta(\tau) \tag{3}$$

where η is a Gaussian noise with zero average and a variance of 2.

Even for a complex action (equivalently complex measure), one can use the same Langevin equation (1) to define a stochastic process. The field gets complexified, and we use the analytically continued drift terms to define $K(x)$ on the complexified manifold [19,20].

In the case of gauge theories our variables will be elements of a Lie group, corresponding to parallel transporters along the links of a cubic space-time lattice. We will be interested in SU(N) gauge theories below, and in particular in $N = 3$ describing the strong interaction sector of the Standard Model. The derivative in the drift term in this case is the left derivative, with respect to the Lie group's generators, such that

$$D_a f(U) = \frac{\partial}{\partial \alpha} f(e^{i\alpha\lambda_a}U)\big|_{\alpha=0}, \tag{4}$$

where λ_a is the ath Gell-Mann matrix for $N = 3$. Defining our gauge theory on a cubic space-time lattice, the drift term for the link variable $U_\nu(x)$ at site x in direction ν is given by

$$K^a_{\nu x} = -D_{\nu x a} S[U]. \tag{5}$$

The discretized Langevin equation becomes

$$U^{\tau+\epsilon}_\nu(x) = \exp\left[i\lambda_a(\epsilon K^a_{\nu x}[U^\tau] + \sqrt{\epsilon}\eta^a_{\nu x}[U^\tau])\right]U^\tau_\nu(x). \tag{6}$$

The use of the exponential update factor ensures that the determinant of the U matrices remain unity; however it is

worth noting that if the action is complex, then the drift term $K^a_{\nu x}[U]$ is also complex. This means the SU(N)-element link variables drift into SL(N, $\mathbb{C}$), as the unitarity is no longer preserved by the update.

A. Boundary terms

One of the failure modes of the complex Langevin simulations is caused by the complexified distributions having a long tail in imaginary directions. This than invalidates the formal proof of correctness [21,23]. The discrepancy of the correct results and complex Langevin results can be understood in terms of boundary terms as follows [28–30]: We define an interpolation function, which for an action depending on a single variable is written as

$$F_{\mathcal{O}}(t,\tau) = \int P(x,y,t-\tau)\exp(\tau L_c)\mathcal{O}(x,y)dxdy, \quad (7)$$

where $P(x,y,t) > 0$ is the distribution of the process on the complexified manifold at Langevin time t, $O(x,y) = O(x+iy)$ is some holomorphic observable, and L_c is the complex Fokker-Planck operator, which (for theories with multiple degrees of freedom) is written as

$$L_c = \sum_i (\partial_i + K_i)\partial_i, \quad (8)$$

where K_i is the drift term of the ith field in the action and ∂_i is derivation with respect to the ith field. The combination $\exp(\tau L_c)\mathcal{O}(x,y)$ thus defines a τ dependent observable. Trivially, $F(t,\tau=0)$ gives the expectation value of observable $\mathcal{O}(x,y)$ in the complex Langevin simulation at Langevin time t. One can show that if one takes a large $\tau = t$, then one has with $\rho = \exp(-S)$

$$F_{\mathcal{O}}(t,t) = \int P(x,y,0)\exp(tL_c)\mathcal{O}(x,y)dxdy = \langle\mathcal{O}\rangle_\rho, \quad (9)$$

where P denotes the probability density produced by CLE, and we have

$$\langle\mathcal{O}\rangle_\rho = \frac{\int dx\mathcal{O}(x)\rho(x)}{\int dx\rho(x)}, \quad (10)$$

i.e., the correct result, assuming the L_c operator has a nondegenerate zero eigenvalue and no eigenvalues with positive real part [21,23]. This spectral requirement is often fulfilled; however there are some known exceptions [27].

We can thus take $F(t,0) - F(t,t)$ as the difference of the CLE result and the correct result. We define the nth boundary term of the observable $\mathcal{O}$ as

$$B_n(\mathcal{O}) = \partial^n_\tau F(t,\tau=0). \quad (11)$$

In practice we mostly check the first boundary term of an observable, and we can take that value as an indicator of the magnitude of the errors of complex Langevin results. To calculate this derivative we need to regularize the observable by an imaginary cutoff,

$$B_1(\mathcal{O},C) = \int dx \int_{-C}^{C} dy P(x,y,0)(L_c\mathcal{O}(x,y)) \quad (12)$$

and measure the observable as an extrapolation to $C\to\infty$. (The boundary term might be undefined or very noisy if one uses directly $C=\infty$.) This procedure is straightforwardly generalizable to lattice systems, where the generalization involves calculating the boundary term observables $L^n_c\mathcal{O}$ using (8), and choosing a cutoff such that a finite C defines a compact manifold incorporating the original real manifold. For simulations using link variables on SU(3), the complexified manifold becomes SL$(3,\mathbb{C})$, and one can use the unitarity norm for the cutoff:

$$N_U = \max_{x,\nu} \mathrm{Tr}[(U_{x\nu}U^\dagger_{x\nu} - 1)^2], \quad (13)$$

such that the boundary term is given by

$$B_n(\mathcal{O},C) = \langle\theta(C - U_N)L^n_c\mathcal{O}\rangle. \quad (14)$$

Note that a nonzero boundary term indicates incorrect results such that the magnitude of the error corresponds to the magnitude of the boundary term. However, in some cases, especially when one uses a kernel in the Langevin equation, one can have incorrect results in spite of the boundary term being zero, which is a consequence of other so-called integration cycles contributing to the result. See the detailed study of this phenomena in [56].

B. Dynamical stabilization

In some cases the large fluctuations of the fields in imaginary directions have been identified to cause wrong convergence of the complex Langevin method. Here we will investigate dynamical stabilization [53], which is essentially a soft cutoff on the distance of the link variables from the original SU(3) manifold. This is achieved by introducing a purely imaginary additional force in the drift term that pushes the variables towards SU(3). This new term in the drift is not a derivative of an action, and moreover it is given by a nonholomorphic function of the complexified fields of the theory. This implies that the argument for correctness of the complex Langevin method no longer applies, indeed our aim is to quantify the bias that this addition imparts on our results. The proposed force is given in [53] as

$$K^a_{x\nu} \to K^a_{x\nu} - i\alpha_{\mathrm{DS}} b^a_x (b^c_x b^c_x)^3 \quad (15)$$

with

$$b_x^a[U] = \mathrm{Tr}\left(\lambda_a \sum_\nu U_{x\nu}^\dagger U_{x\nu}\right) \tag{16}$$

such that the force is zero if the gauge links are SU(3) elements, and preserves the gauge symmetry with respect to SU(3) gauge transformations. Notice that, in $(b_x^c b_x^c)$, the sum over the Gell-Mann matrices can be simplified using the Fierz completeness relation of the generators for SU(N), giving

$$b_x^c[U]b_x^c[U] = 2\mathrm{Tr}\left(\sum\nolimits_\nu U_{x\nu}^\dagger U_{x\nu}\right)^2 - \frac{2}{3}\mathrm{Tr}^2\left(\sum_\nu U_{x\nu}^\dagger U_{x\nu}\right). \tag{17}$$

The parameter α_{DS} controls the strength of the force and we will show results for multiple orders of magnitude of α_{DS}, to get insight in this parameter's effect on the simulation. In addition we also investigate a slightly different dynamical stabilization force, which does not sum over the directions, to keep the force on link variables in different directions independent.

$$K_{x\nu}^a \to K_{x\nu}^a - i\alpha_{\mathrm{DS}} b_{x\nu}^a (b_{x\nu}^c b_{x\nu}^c)^3, \tag{18}$$

using

$$b_{x\nu}^a[U] = \mathrm{Tr}(\lambda_a U_{x\nu}^\dagger U_{x\nu}), \tag{19}$$

which we call the nonmixing version of the DS force below. Also in this case one can use the Fierz completeness relations to simply the terms in the bracket:

$$b_{x\nu}^c[U]b_{x\nu}^c[U] = 2\mathrm{Tr}(U_{x\nu}^\dagger U_{x\nu})^2 - \frac{2}{3}\mathrm{Tr}^2(U_{x\nu}^\dagger U_{x\nu}). \tag{20}$$

In the numerical simulations we use adaptive step sizes, such that the norm of the drift term times the step size is not allowed to grow too large. We ensure this condition is satisfied after the dynamical stabilization term has been added to the drift.

C. One-link toy model

Before simulating full QCD, we will investigate a simple one-plaquette model called Polyakov chain [37], here with only one link variable $U \in \mathrm{SU}(3)$ representing the Polyakov loop, with the action

$$-S = \beta_1 \mathrm{Tr}U + \beta_2 \mathrm{Tr}U^{-1} \tag{21}$$

and

$$\beta_1 = \beta + \kappa\exp(\mu), \qquad \beta_2 = \beta + \kappa\exp(-\mu). \tag{22}$$

Here β and κ are coupling constants, and μ is the chemical potential. Furthermore the drift term can be calculated to be

$$K_a = i\beta_1 \mathrm{Tr}(\lambda_a U) - i\beta_2 \mathrm{Tr}(\lambda_a U^{-1}), \tag{23}$$

using the left derivative described in Eq. (4). We then add the dynamical stabilization to the drift,

$$\begin{aligned} M_a &= K_a - S_a, \\ S_a &= i\alpha_{\mathrm{DS}} d^3[U]\mathrm{Tr}(\lambda_a U^\dagger U), \end{aligned} \tag{24}$$

with

$$d[U] = 2\mathrm{Tr}(U^\dagger U)^2 - \frac{2}{3}\mathrm{Tr}^2(U^\dagger U), \tag{25}$$

and thus we use M_a instead of K_a in the Langevin update Eq. (6).

For this model we have then found values for β, κ, and μ, such that the model gives incorrect convergence without the use of dynamical stabilization. The observables considered here are the trace of the Polyakov loop $P = \mathrm{Tr}U$, and the trace of the inverse Polyakov loop $P' = \mathrm{Tr}U^{-1}$, which is then compared to the exact value. The exact values are found by numerically integrating over conjugacy classes of the SU(3) group [57], such that the Polyakov loop is represented by a diagonal matrix $\mathrm{diag}(e^{i\phi_1}, e^{i\phi_2}, e^{-i(\phi_1+\phi_2)})$ using the reduced Haar measure of the conjugacy classes

$$\begin{aligned} dU = \sin^2\left(\frac{1}{2}\phi_1 + \phi_2\right)\sin^2\left(\phi_1 + \frac{1}{2}\phi_2\right)\cdot \\ \times \sin^2\left(\frac{\phi_1 - \phi_2}{2}\right)\frac{d\phi_1 d\phi_2}{N}, \end{aligned} \tag{26}$$

where N is a normalizing factor, and $-\pi < \phi_1, \phi_2 \leq \pi$ are the two free variables parametrizing the conjugacy classes. This measure can be used in numerical integrations of the expectation values for P and P' using, e.g., the trapezoidal rule.

D. QCD

The full-QCD simulations use the Wilson plaquette action for the gauge degrees of the freedom and $N_F = 4$ species of staggered fermions (if not noted otherwise). (For the definition of the Wilson plaquette action as well as a general introduction into lattice QCD, see, e.g., [58]. Our observables are also defined in the results section.)

The contribution of the gauge degrees of freedom to the drift terms is calculated straightforwardly from the action. [It is worth noting that writing the plaquette action one uses U^{-1} instead of $U^\dagger$, to preserve the holomorphicity of the action. While for SU(N) this would be equivalent, extending the process to SL(N, $\mathbb{C}$), it becomes a crucial distinction.] We use gauge cooling to avoid the fast blowup of the unitarity norm, enabled by the complexified gauge degrees of freedom [37,38]. The contribution of the fermions to the ath color component of the drift term of

the link at site x, pointing in direction ν is written as

$$K^F_{x\nu a} = \frac{N_F}{4}\mathrm{Tr}(M^{-1}D_{x\nu a}M), \tag{27}$$

with the Dirac matrix M, which for unimproved staggered fermions reads as

$$M_{xy} = m\delta_{xy} + \sum_\nu \eta_\nu(x)[e^{\delta_{\iota 0}\mu}U_\nu(x)\delta_{x+\hat{\nu},y} - e^{-\delta_{\iota 0}\mu}U^{-1}_\nu(y)\delta_{x-\hat{\nu},y}] \tag{28}$$

with the staggered phases $\eta_\nu(x)$. The trace in the drift term is calculated using the noisy estimator [43] to avoid having to calculate the inverse of the Dirac matrix M^{-1}. For small lattices the calculation of the inverse of the Dirac matrix is affordable (using, e.g., the LU decomposition), so in some cases we calculate the exact fermionic drift terms using the exact M^{-1}. While more expensive, exact drift terms are beneficial as they allow for simulations at lower inverse gauge coupling (β) values, because the lack of the noise in the drift terms results in more stable simulations.

III. RESULTS

A. One-link toy model results

In this section we first show numerical results for the toy model defined in Eq. (21). We used an adaptive Langevin update with a maximum step size of $\Delta\tau = 10^{-4}$. We typically used $\tau = 100$ Langevin time for thermalization, and we used further $\tau = 10^5$ for measuring the averages. To calculate the error bars we used the bootstrap procedure after binning the data to get rid of the autocorrelations of the process. We chose $\beta = 0.1$, $\kappa = 0.25$, and $\mu = 1.0$, which is a point where the complex Langevin method gives slightly incorrect results. At larger β and lower κ it gives correct results and thus dynamical stabilization is not needed.

We first test the dependence of the results on the control parameter of the dynamical stabilization α_{DS} in Fig. 1. We show the numerically integrated exact results as well as the phase quenched exact value (PQ), which is calculated by taking the absolute value of the measure in the expectation value:

$$\langle P\rangle_{\mathrm{PQ}} = \frac{1}{Z_{\mathrm{PQ}}}\int Pe^{-\mathrm{Re}S(U)}dU,$$
$$Z_{\mathrm{PQ}} = \int e^{-\mathrm{Re}S(U)}dU. \tag{29}$$

The behavior of the process changes qualitatively if α_{DS} is changed over a large range of magnitudes; therefore we plot results on a logarithmic α_{DS} scale. We first note that at $\alpha_{\mathrm{DS}} = 0$ the complex Langevin results are incorrect; we have checked that this is correctly signaled also by nonzero

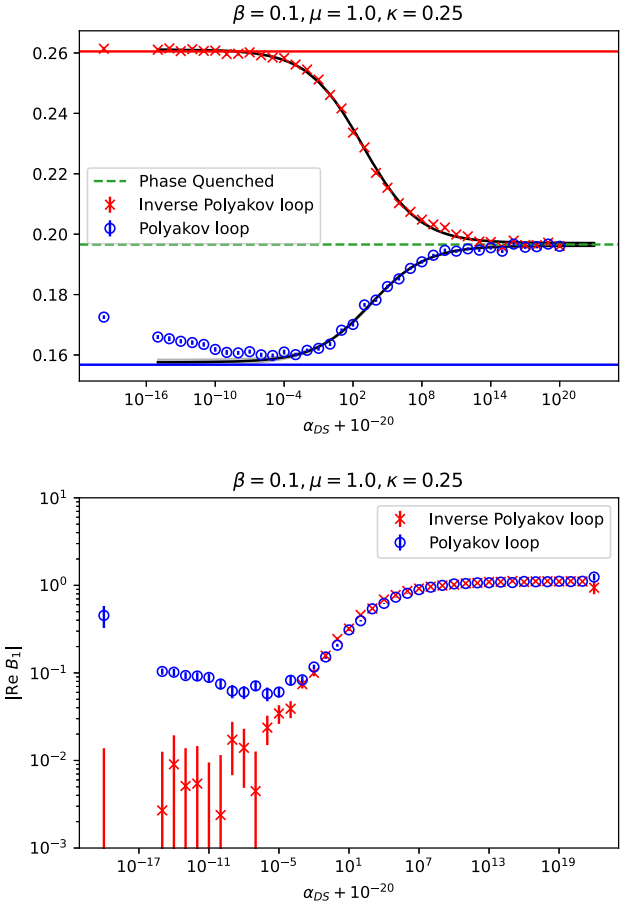

FIG. 1. Above, the Polyakov loop P and the inverse Polyakov loop P' are shown in the toy model (21) at $\beta = 0.1$, calculated using dynamically stabilized CLE, as a function of the α_{DS} parameter. The exact results calculated by numerical integration (red/blue lines) and the phase quenched exact result (green line) is also shown, as well as a fitted sigmoid curve, defined in (30) (dark gray line with error bands). Below, the absolute values of the boundary terms are shown for the Polyakov loop and the inverse Polyakov loop variable as a function of α_{DS}. Note that we added 10^{-20} to α_{DS} to allow $\alpha_{\mathrm{DS}} = 0$ to appear on the logarithmic x axis.

boundary terms, as is visible on the second plot of Fig. 1. At large α_{DS} the link variable has a strong force pushing it back towards the SU(3) manifold. It is expected that, in the limit of very large α_{DS}, the link variable will be confined to the SU(3) manifold and its dynamics will be given by that of phase quenched theory, as the real parts of the drift term are calculated from the action, and the imaginary parts are rendered mute by the dynamical stabilization term. In the phase-quenched theory the real part of the Polyakov loop and its inverse are equal, as the link variable is unitary. This behavior is nicely observed in the numerical experiments, as visible in Fig. 1. Also noteworthy is the fact that even though the CLE results are incorrect at $\alpha_{\mathrm{DS}} = 0$, introducing a moderate value for α_{DS} actually drives the results closer to the exact value, before finally they approach the

TABLE I. Comparison of the exact values, CLE results extrapolated to $\alpha_{\mathrm{DS}} = 0$, and CLE results of simulations at $\alpha_{\mathrm{DS}} = 0$.

	$\langle U \rangle$	$\langle U^{-1} \rangle$
Exact	0.1567728	0.2605116
Extrapolated	0.15756(94)	0.26113(25)
CLE $\alpha_{\mathrm{DS}} = 0$	0.17254(61)	0.26139(62)

phase-quenched value. The α_{DS} dependence of the results is well described by a sigmoid dependence if we exclude the small α_{DS} region. We have fitted the data with a four parameter fit using the function

$$f(\alpha_{\mathrm{DS}}) = A + \frac{B - A}{1 + C\alpha_{\mathrm{DS}}^{D}}. \tag{30}$$

For the fit we only used simulation values at $\alpha_{\mathrm{DS}} \geq 10^{-5}$. [Not knowing the exact results, one could justify this by the nonmonotonic behavior as a function of α_{DS} or the increase of the boundary terms, as well as the increase in the R ratio (defined below).] The quality of the fit can be judged from $\chi^2/n_{\mathrm{d.o.f.}} \approx 1$–3 for this fitting range. As observed in Fig. 1, the fit function extrapolated to $\alpha_{\mathrm{DS}} = 0$ gives the correct results with good accuracy, as is also visible in Table I. Notably, for the parameter D (the exponent of α_{DS} in the sigmoid function), we get a value close to 0.25.

In Fig. 2 we show the unitarity norm

$$N_U = \mathrm{Tr}[(UU^\dagger - 1)^2] \tag{31}$$

as well as the ratio of norms of the dynamical stabilization term versus the drift term coming from the action

$$R = \frac{\sqrt{\langle \sum_a |S_a|^2 \rangle}}{\sqrt{\langle \sum_a |K_a|^2 \rangle}}. \tag{32}$$

This gives information on how much the stabilization changes the original drift terms of the theory. The magnitude of the norm of K_a is approximately independent of α_{DS} so the ratio roughly corresponds to the norm of S_a. (For very small α_{DS} values the system is instable and thus the magnitude of drift terms increase when one is in the instable region or close to it). We observe that this ratio has a minimum in the investigated α_{DS} range, as for small α_{DS} the fields deviate more from SU(3), and thus the attractive force towards SU(3) tends to be larger. For large α_{DS} the force increases again as it is multiplied by a factor α_{DS}. Note that the minimum of this ratio roughly coincides with the α_{DS} value which corresponds to minimal boundary terms, as visible in Fig. 1. We also carried out simulations at $\beta = 1.0$, where the CLE simulations with $\alpha_{\mathrm{DS}} = 0$ already gave a correct result. A small stabilization force does not spoil this, but a too large α_{DS} drives the results to the

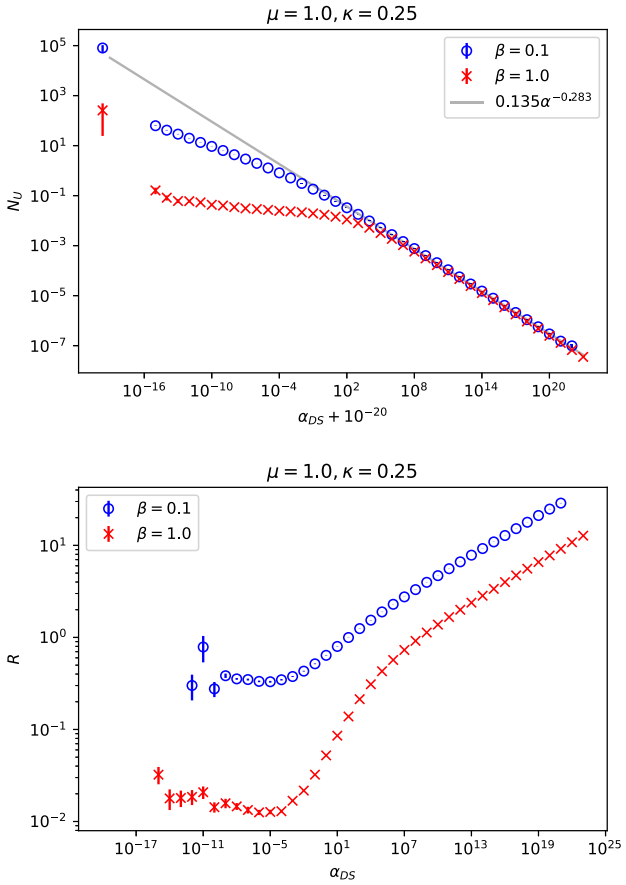

FIG. 2. The unitarity norm as well as a the ratio of the norm of the drift terms coming from the action vs the norm of the dynamical stabilization force [defined in (32)] as a function of α_{DS} for the toy model.

phase-quenched values, as visible in Fig. 3. At $\beta = 1.0$ both the direct simulation and the extrapolation to $\alpha_{\mathrm{DS}} = 0$ from simulations above $\alpha_{\mathrm{DS}} = 10^{-5}$ (where R has a minimum) give results which are consistent with exact results within statistical errors. For simulations at $\beta = 1.0$ we got $\chi^2/n_{\mathrm{d.o.f.}} \approx 1$–1.3, showing that the α_{DS} dependence is well described by the ansatz. At lower α_{DS} values for $\beta = 1.0$, the unitarity norm levels off at a certain value, as the distribution is constrained by the complexified stochastic process and not by the stabilizing force, as observed in Fig. 2. At high α_{DS}, the decay of the unitarity norm follows a power law behavior with the exponent ≈ -0.28, which is close to the value $1/4$, which can be understood as the "thermal" average that corresponds to the rough structure of the dynamical stabilization term in the following sense: close to the real manifold and linearizing using $U = U_0 e^{\gamma_a \lambda_a}$ with $\gamma_a \ll 1$ and $U_0 \in \mathrm{SU}(3)$ we can define the DS action as $S_{\mathrm{DS}} = (\sum_a \gamma_a^2)^4$. The derivative of this action is than (to first order in γ) the DS term used above (note that the actual dynamical stabilization term defined in Sec. II B. is not the derivative of an action). The unitarity norm in this approximation is $UN \sim \gamma_a^2$. A thermal average then gives

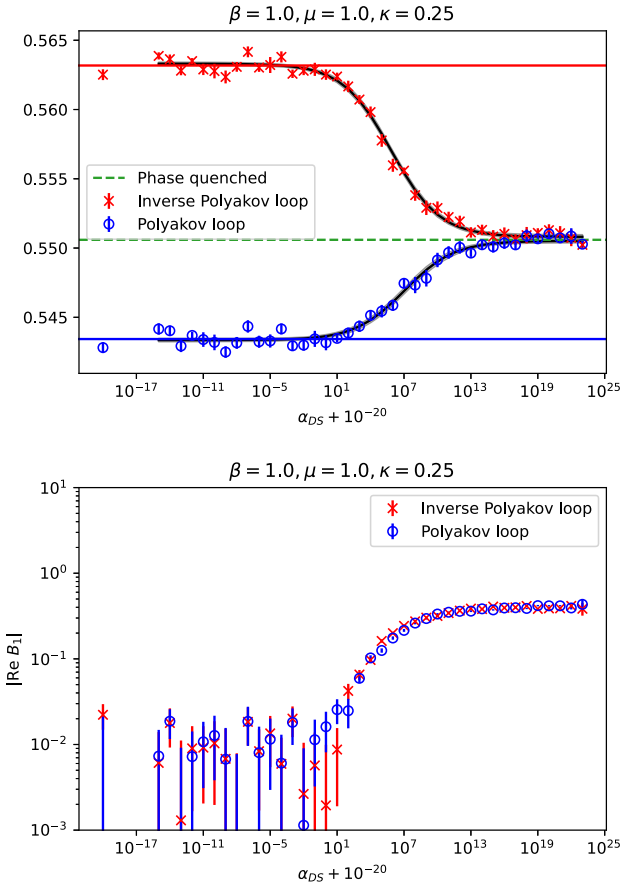

FIG. 3. Above, the Polyakov loop P and the inverse Polyakov loop P' are shown in the toy model (21) at $\beta = 1.0$, calculated using dynamically stabilized CLE, as a function of the α_{DS} parameter. The exact results and the phase quenched result, are also shown (full lines). Below, the absolute value of the boundary terms are shown for the Polyakov loop and the inverse Polyakov loop variable as a function of α_{DS}.

$$\langle N_U \rangle \sim \frac{1}{Z} \int \gamma^2 e^{-\alpha_{\mathrm{DS}} \gamma^8} \, d\gamma \sim \alpha_{\mathrm{DS}}^{-1/4} \tag{33}$$

with the normalization $Z = \int \exp(-\alpha_{\mathrm{DS}} \gamma^8) d\gamma \sim \alpha_{\mathrm{DS}}^{-1/8}$. This simple model can capture most of the α dependence; however, since the evolution of the link variables is not governed by imaginary noise terms (instead, the drift terms have imaginary parts), and thus a thermal average is at best an approximation. For these reasons, this model is not expected to be exact and, as one observes, the exponent is slightly different from $1/4$.

The boundary terms also confirm correct results at small α_{DS} values; however at large α_{DS} they signal the incorrect results as the large dynamical stabilization force spoils the correspondence of the complex Langevin process and the original complex measure.

The results in this section are qualitatively similar to our results in QCD at high temperature to be discussed in the next section.

B. QCD results

Next we turn to results of simulations of full QCD. We used simulations on $8^3 \times 4$ lattices (unless otherwise noted) using the plaquette action for the gauge fields and $N_F = 4$ flavors of unimproved staggered fermions using $m = 0.02$ (in lattice units). To test different temperatures and thus different phases of the theory we change the β parameter of the gauge action. After performing a β scan to explore the qualitative behavior of the dynamical stabilization force, we used $\beta = 4.9$ for simulations in the deconfinement region and $\beta = 5.2$ for simulations in the confinement region. (The critical inverse coupling on the $8^3 \times 4$ lattice using the parameters mentioned above and $\mu = 0$ is roughly $\beta_c \approx 5.0$.)

We use a nonzero chemical potential μ to induce a sign problem. In the standard reweighting method, one can express averages at nonzero μ with averages measured at $\mu = 0$ by pushing the oscillating part of the measure (contributed by the fermionic determinant) into the observable

$$\begin{aligned}
\langle F[U] \rangle_\mu &= \frac{\int DU F[U] e^{-\beta S_G[U]} \det M[U,\mu]}{\int DU e^{-\beta S_G[U]} \det M[U,\mu]}, \\
&= \frac{\int DU F[U] e^{-\beta S_G[U]} \det M[U,\mu=0] \frac{\det M[U,\mu]}{\det M[U,\mu=0]}}{\int DU e^{-\beta S_G[U]} \det M[U,\mu=0] \frac{\det M[U,\mu]}{\det M[U,\mu=0]}}, \\
&= \left\langle F[U] \frac{\det M[U,\mu]}{\det M[U,\mu=0]} \right\rangle_{\mu=0} \Bigg/ \\
&\quad \left\langle \frac{\det M[U,\mu]}{\det M[U,\mu=0]} \right\rangle_{\mu=0},
\end{aligned} \tag{34}$$

where DU is a shorthand for an integral over all the link variables of the lattice, $S_G[U]$ is the action of the gauge fields and $M(U,\mu)$ is the fermionic matrix. This approach fails at large μ because statistical errors blow up, as both averages to be measured for the above formula become close to zero, and also an overlap problem develops (the distribution of the reweighting weights becomes very non-Gaussian). For further details of the reweighting method see, e.g., [59] and references therein. For this study we use a relatively small quark chemical potential $\mu = 0.1$ (in lattice units), that is in a region where one can still calculate reweighted results with a reasonable effort with relatively small errors. For the reweighting we used about 22 000 configurations for $\beta = 4.9$ and 6000 configurations for $\beta = 5.2$, which we collected using a Hybrid Monte Carlo (HMC) procedure at $\mu = 0$ and the respective gauge couplings $\beta = 4.9$ and $\beta = 5.2$. To calculate the ratio of the determinants for reweighting we used a decomposition of the staggered determinant found in [60], which reduces the size of the fermionic matrix by a factor of $N_t/2$. Since in this μ region the reweighting produces exact results, we have

opted not to calculate boundary terms in the QCD simulations for this study, but they deserve to be the subject of a future study, especially to investigate the effect of the stabilization on the boundary terms. See [61] for a previous calculation of boundary terms in QCD. We note that including dynamical stabilization has in practice no effect on the feasibility of the boundary term calculations, so such calculations are within reach of the typical computational budget of lattice simulations of CLE.

We used complex Langevin simulations with adaptive step-size control to get rid of the runaway trajectories [22]. The simulations are started from a random initial SU(3) configuration, and we use a $\tau = 10$ Langevin time period for thermalization and we measure observables for a further $\tau = 90$ Langevin time. Our main observables are the plaquette average

$$U_{\alpha\beta} = \frac{1}{N_s^3 N_t} \sum_x U_{x,\alpha} U_{x+\hat{\alpha},\beta} U^{-1}_{x+\hat{\beta},\alpha} U^{-1}_{x,\beta}, \tag{35}$$

the Polyakov loop and its inverse

$$P = \frac{1}{N_s^3} \sum_x \mathrm{Tr}\left(\prod_{\tau=0}^{N_\tau - 1} U_{x+\tau\hat{0},0} \right), \tag{36}$$

$$P' = \frac{1}{N_s^3} \sum_x \mathrm{Tr}\left(\prod_{\tau=N_\tau-1}^{0} U^{-1}_{x+\tau\hat{0},0} \right), \tag{37}$$

as well as the fermionic observables: the chiral condensate

$$\chi = \frac{1}{\Omega} \frac{\partial \ln Z}{\partial m} = \frac{N_F}{4\Omega} \mathrm{Tr}(M^{-1}) \tag{38}$$

and the baryonic density

$$n_B = \frac{1}{\Omega} \frac{\partial \ln Z}{\partial \mu} = \frac{N_F}{4\Omega} \mathrm{Tr}(M^{-1} \partial_\mu M). \tag{39}$$

with the dimensionless space-time volume $\Omega = N_s^3 N_t$. We also measure the ensemble average of the maximal unitarity norm on the lattice:

$$N_U = \max_{x,\nu} \mathrm{Tr}[(U_{x\nu} U_{x\nu}^\dagger - 1)^2]. \tag{40}$$

$N_U \geq 0$ is not a physical observable, it monitors how far the link variables are from the SU(3) manifold [we have $N_U = 0$ for an SU(3) configuration].

To get a broad overview of the effect of dynamical stabilization we first performed simulations on 4^4 lattices. For these simulations we used an exact drift force for the fermionic drift terms (instead of the noisy estimator described in [43]). The exact drift terms allow for simulations at low β values also at small α_{DS} values, but the numerical costs are considerably higher [62], therefore we

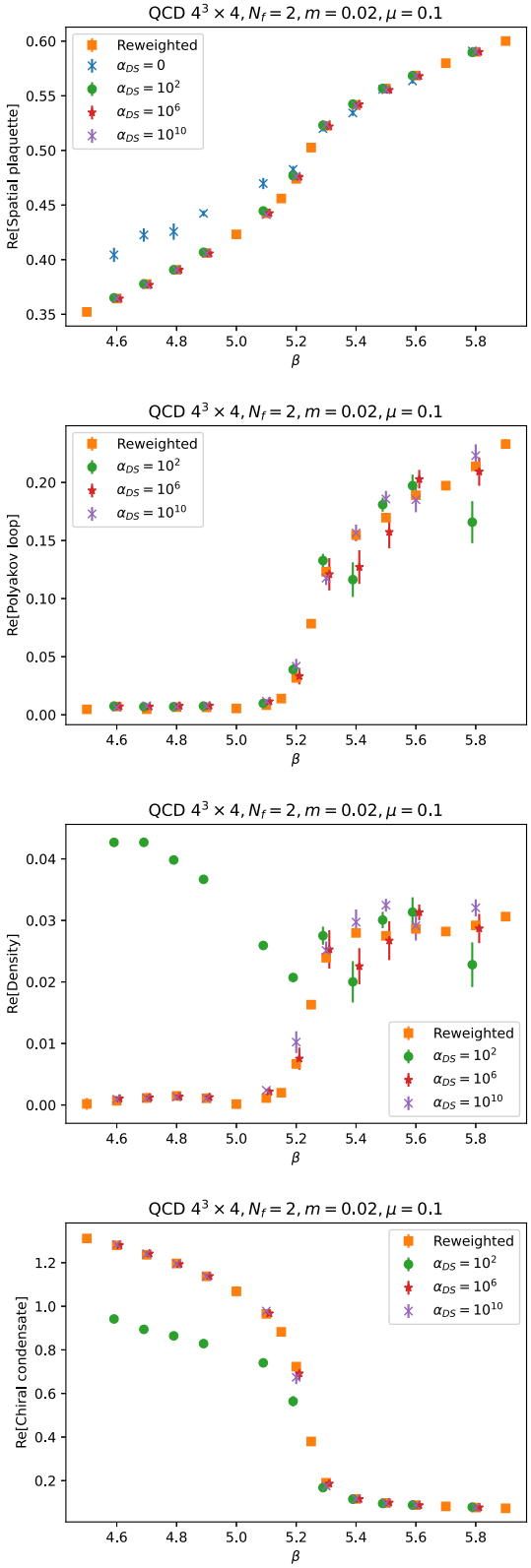

FIG. 4. Various observables (spatial plaquette, Polyakov loop, chiral condensate, baryonic density) as a function of the inverse gauge coupling beta β for QCD simulations on a 4^4 lattice, for various dynamical stabilization parameters, as indicated.

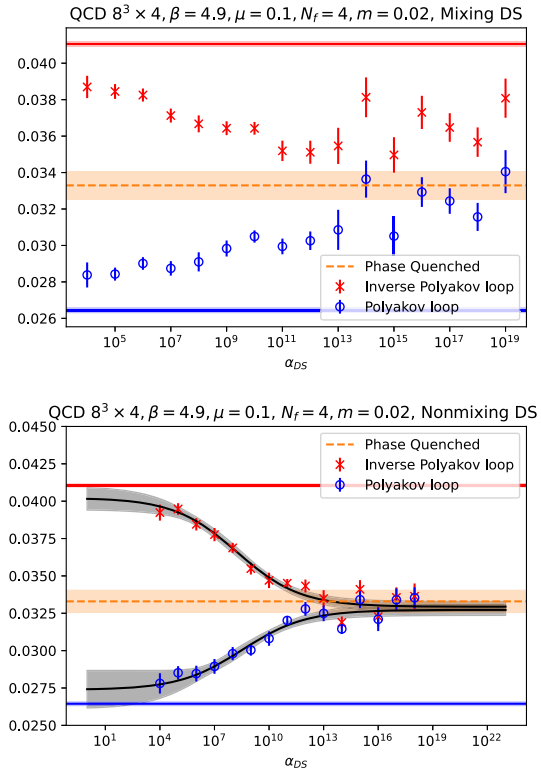

FIG. 5. The Polyakov loop P and its inverse P' in QCD simulations in the low temperature, confined phase of the theory at $\mu = 0.1$. Lines represent results reweighted from $\mu = 0$. Also shown is the phase quenched result. The CLE simulations use the mixing formulation (15) of the dynamical stabilization force above, and the nonmixing (18) below.

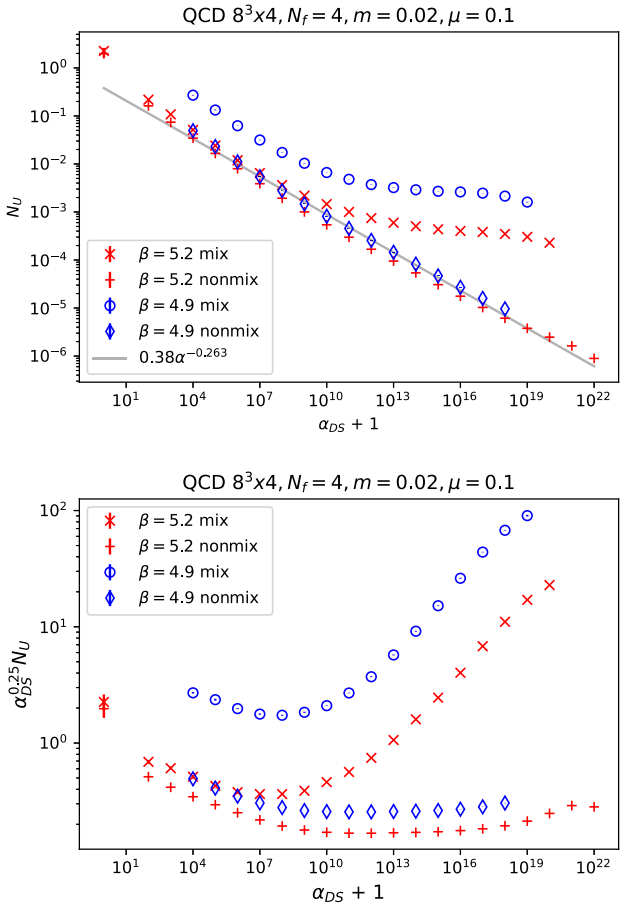

FIG. 6. The unitarity norm as a function of α_{DS} in QCD simulations at low temperatures (blue symbols) and high temperatures (red symbols). Two versions of the dynamical stabilization force are used, as indicated. Below, the average unitarity norm rescaled with $\alpha_{\mathrm{DS}}^{0.25}$, as indicated.

restricted the lattice size to 4^4. (The noisy estimator at low β without substantial stabilization leads to instable simulations.) In Fig. 4 we show the plaquette average as well as the Polyakov loop, chiral condensate, and the baryonic density. We observe that no stabilization or not enough stabilization at low β values gives incorrect results for all observables, while at high β (corresponding to high temperatures) we see correct results. Introducing the stabilization, we get seemingly correct results also at low β. Next, we precisely calculate the observables on a larger lattice ($8^3 \times 4$) to see if there is some small bias remaining, caused by the nonholomorphic stabilization force.

In Fig. 5 we show results from the low temperature phase of the theory. In this phase the CLE simulations at $\alpha_{\mathrm{DS}} = 0$ (or too small α_{DS}) tend to be instable, and introducing a small α_{DS} allows for long simulations.

One observes that for moderate α_{DS} the results are close to the exact results for both versions of the stabilizing force, but in the case of the inverse Polyakov loop we see statistically significant differences. At large α_{DS} the results get nearer to the phase-quenched values, as expected. We note that the nonmixing dynamical stabilization seems to present a stronger push towards the real manifold, as we observe that for larger α_{DS} the Polyakov loop and the inverse Polyakov loop are approximately equal, signaling that the link variables are close to the SU(3) manifold, such that effectively we simulate the phase-quenched system. This is confirmed by Fig. 6, where the average unitarity norm is shown as a function of α_{DS}. We note that at very large α_{DS} the simulation times increase as the dynamical stabilization force gets higher and in turn the adaptively controlled Langevin step size can get very small. Intuitively the weakness of the mixing version is understood such that the force towards the real manifold is weakened, because the forces of the different directions are effectively averaged over. In Fig. 7 we show the comparison of the Polyakov loops with reweighting results for high temperature, above the deconfinement transition for $\mu = 0.1$. In this phase the simulation already at $\alpha_{\mathrm{DS}} = 0$ supplies results consistent with the exact results; i.e., dynamical stabilization is not needed. If one uses a too high α_{DS}, then the results get close to the phase-quenched results, as expected. We fit the results using the sigmoid ansatz (30), and we get relatively good quality fits with $\chi^2/n_{\mathrm{d.o.f.}} \approx 1$–2.3. In Fig. 8 we show the ratio of the norms of the "normal" drift terms coming from the

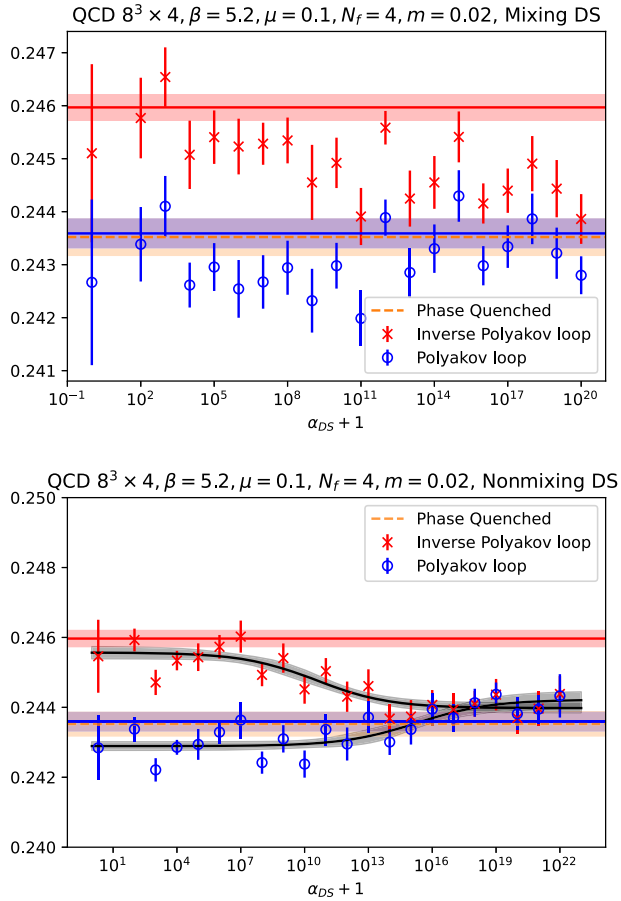

FIG. 7. The Polyakov loop P and its inverse P' in QCD simulations in the high temperature, deconfined phase of the theory, at $\mu = 0.1$. Lines represent results reweighted from $\mu = 0$. Also shown is the phase quenched result. The CLE simulations use the mixing formulation (15) of the dynamical stabilization force above and the nonmixing (18) below.

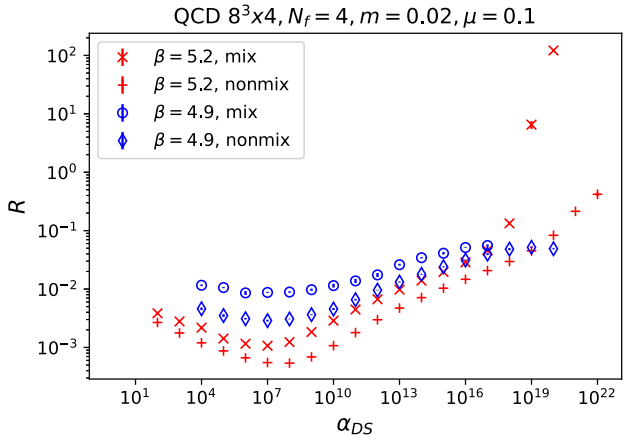

FIG. 8. The ratio of the norm for the drift terms coming from the action and the stabilizing force [defined in (32)] in the QCD simulations is shown as a function of α_{DS} in QCD simulations at different temperatures and two versions of the dynamical stabilization force are used, as indicated.

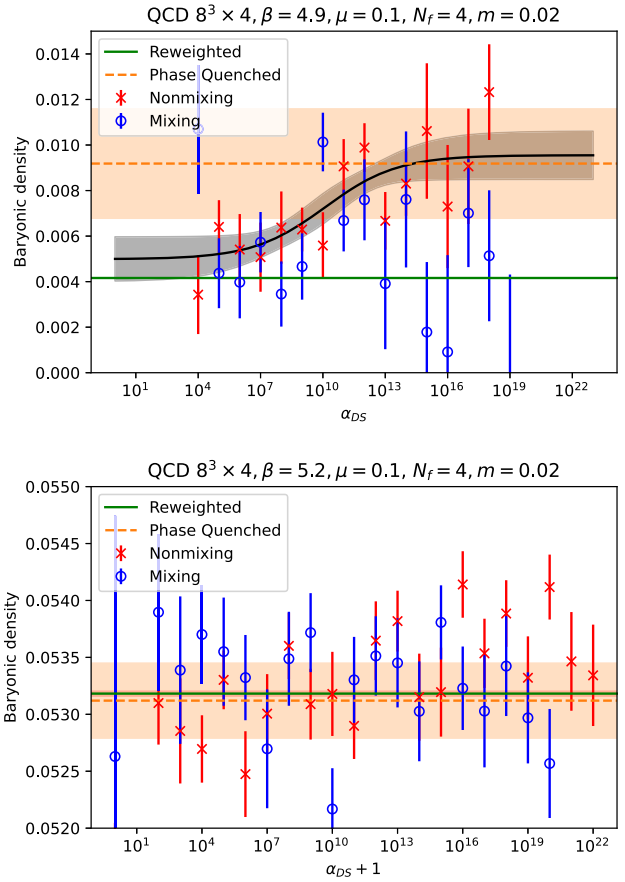

FIG. 9. The baryonic density in QCD simulations at low temperatures (above) and high temperatures (below) as a function of α_{DS}. The low temperature CLE results with nonmixing stabilization (red symbols) are fitted with a sigmoid curve (30), where we have kept the D parameter at a fixed value $D = 0.25$.

action and the dynamical stabilization force, as defined in (32). The norm of the "normal" part of the drift is roughly independent of α_{DS}, so this ratio essentially measures how large the stabilization forces are. First of all, we see that the ratio is always relatively small, meaning that the dynamical stabilization is indeed a small correction to the drift. This is especially true for high temperatures, where simulations without stabilization can work as well. For lower temperatures the stabilizing force gets relatively larger, but they are at least an order of magnitude smaller than the force coming from the action (for not too large α_{DS} values). One also observes generally larger stabilization terms for the mixing stabilization; this is a consequence of the slightly more spread out distribution for the mixing stabilization for a given α_{DS}, as observed in Fig. 6.

Finally we note that for the nonmixing stabilization force the decay of the average unitarity norm as α_{DS} is increased is approximately described by a power law dependence $N_U \sim \alpha_{\mathrm{DS}}^{-0.25}$. For the mixing version this dependence is more complicated, the rate of decay gets diminished for large α_{DS}, as visible in Fig. 6.

In Fig. 9 we show the fermionic density. At low temperatures we can see a small effect of the phase quenching, and the simulation values follow the sigmoid fit for the nonmixing version of the stabilization force. (For the fit we had to fix the parameter D to the value $D = 0.25$, to let the fit converge in spite of the biasing effect being in the same order of magnitude as the error bars of the observable.) At high temperatures at the chemical potential we used here there is no significant difference between the phase quenched and the reweighted density. Similarly, when investigating the chiral condensate one observes that the CLE simulations, the reweighted results and the phase-quenched results are consistent with each other within the statistical precision we have.

IV. CONCLUSIONS

In this paper we have investigated the proposed dynamical stabilization force for the complex Langevin simulations of QCD. We introduced a second version of the stabilizing force that does not mix together the forces on the links pointing to the different directions attached to the same lattice point but deals with each link separately. The strength of the force pushing the fields towards the SU(3) manifold is controlled by the parameter α_{DS}. This parameter needs to be changed over many orders of magnitude to change the behavior of the stabilized system qualitatively, so results are considered to be dependent on the logarithm of α_{DS}.

As the stabilizing force is an *ad hoc* addition to the drift term in the Langevin equation, this breaks the action principle and holomorphy as well. Such a change is expected to spoil the correspondence between the original ensemble on the real manifold and the complex Langevin results. First we investigated the effects of dynamical stabilization on a one-link toy model to gain insight in the qualitative behavior of the system. We observed that the effect of the stabilizing force can be understood as a soft cutoff, such that increasing the control parameter of the stabilizing force does eventually confine the system to the real SU(3) manifold, which is then equivalent to phase quenching. We observed that the functional behavior of the results for varying α_{DS} is well described by a sigmoid fit, in a range where the stabilization of the system is not too weak. The fit function can then be extrapolated to zero stabilization which gives results consistent with the exact results of the system, in spite of CLE simulations at $\alpha_{\mathrm{DS}} = 0$ giving incorrect results for some parameter values of the action of the model.

Next we investigated QCD simulations with four degenerate flavors of staggered fermions. For the simulations we chose a moderate chemical potential such that results can be compared to reweighting. At high temperatures, simulations at $\alpha_{\mathrm{DS}} = 0$ already bring results consistent with the reweighted ones (as observed also in [45]). Simulations with a substantial α_{DS} drive the system towards the phase-quenched system. Smaller α_{DS} might be used to improve the stability of the simulations somewhat (such that larger step sizes are also usable), and the small biasing might be removed with a sigmoid fit similar to the toy model if the nonmixing version of the stabilization is used.

At low temperatures, CLE simulations become instable and break down when the unitarity norm gets O(1). A nonzero α_{DS} makes stable simulations possible also in this regime. However, in this regime the DS force gives a small but nonzero bias in the results of the simulations, which increases as α_{DS} is increased. As expected, the results eventually are driven to the phase-quenched results. The original, mixing version of the stabilization force appears weaker, and numerical problems prevent simulations at very high α_{DS} values (too small step sizes would be needed), such that only a trend towards the phase-quenched results is visible. For the second, nonmixing version of the stabilizing force, similarly to high temperatures, a clean transition to the phase-quenched results is visible and the behavior of the system is well described with a sigmoid fit. Extrapolating to zero stabilization removes most of the bias with respect to the exact results.

In summary, we have shown that the dynamical stabilization is a very useful tool for complex Langevin simulations. For a toy model its effect on the system is well understood and extrapolation to zero stabilization gives correct results. We also studied application of the method to QCD, where we introduced a slightly modified stabilization force, the behavior of which is very similar to the toy-model results, such that extrapolation to zero stabilization was feasible. Since at the moment the complex Langevin method is the only feasible *ab initio* method that works at large chemical potentials, a direct check of its results is only possible in the reach of other methods at small μ. At low temperatures, a good check for consistency is the investigation of the Silver-Blaze phenomenon [63]. Previous studies of the complex Langevin method suggest mild volume dependence on the feasibility of the method, rather, lattice parameters (quark masses, number of flavors, and most importantly β) play an important role. In [52] the authors argue that the bottleneck at lower temperatures and smaller pion masses might be the inversion of the Dirac matrix, so a good regularizing term in the Fermion matrix for complex Langevin simulations limiting the condition number is needed. Further studies will be undertaken to calculate results in QCD extending the temperature range at (or at least closer to) the physical point on larger lattices.

ACKNOWLEDGMENTS

We thank Michael Mandl for his comments on the manuscript. D. S. acknowledges the support of the Austrian Science Fund (FWF) through the Stand alone Project No. P36875. The computational results presented have been achieved in part using the Vienna Scientific Cluster (VSC), and in part on the computing cluster of the University of Graz (GSC).

[1] I. M. Barbour, S. E. Morrison, E. G. Klepfish, J. B. Kogut, and M.-P. Lombardo, Nucl. Phys. B, Proc. Suppl. **60**, 220 (1998).
[2] Z. Fodor and S. D. Katz, J. High Energy Phys. 03 (2002) 014.
[3] M. Giordano, K. Kapas, S. D. Katz, D. Nogradi, and A. Pasztor, J. High Energy Phys. 05 (2020) 088.
[4] C. R. Allton, S. Ejiri, S. J. Hands, O. Kaczmarek, F. Karsch, E. Laermann, C. Schmidt, and L. Scorzato, Phys. Rev. D **66**, 074507 (2002).
[5] R. V. Gavai and S. Gupta, Phys. Rev. D **78**, 114503 (2008).
[6] S. Borsanyi, Z. Fodor, S. D. Katz, S. Krieg, C. Ratti, and K. Szabo, J. High Energy Phys. 01 (2012) 138.
[7] A. Bazavov *et al.*, Phys. Rev. D **95**, 054504 (2017).
[8] P. de Forcrand and O. Philipsen, Nucl. Phys. **B642**, 290 (2002).
[9] M. D'Elia and M.-P. Lombardo, Phys. Rev. D **67**, 014505 (2003).
[10] P. Cea, L. Cosmai, and A. Papa, Phys. Rev. D **89**, 074512 (2014).
[11] R. Bellwied, S. Borsanyi, Z. Fodor, J. Günther, S. D. Katz, C. Ratti, and K. K. Szabo, Phys. Lett. B **751**, 559 (2015).
[12] Z. Fodor, S. D. Katz, and C. Schmidt, J. High Energy Phys. 03 (2007) 121.
[13] G. Endrodi, Z. Fodor, S. D. Katz, D. Sexty, K. K. Szabo, and C. Torok, Phys. Rev. D **98**, 074508 (2018).
[14] A. Alexandru, M. Faber, I. Horvath, and K.-F. Liu, Phys. Rev. D **72**, 114513 (2005).
[15] S. Kratochvila and P. de Forcrand, Proc. Sci. LAT2005 (**2006**) 167 [arXiv:hep-lat/0509143].
[16] C. Gattringer, Proc. Sci. LATTICE2013 (**2014**) 002 [arXiv:1401.7788].
[17] C. Gattringer and K. Langfeld, Int. J. Mod. Phys. A **31**, 1643007 (2016).
[18] J. N. Guenther, Eur. Phys. J. A **57**, 136 (2021).
[19] J. R. Klauder, Acta Phys. Austriaca Suppl. **25**, 251 (1983).
[20] G. Parisi, Phys. Lett. **131B**, 393 (1983).
[21] G. Aarts, E. Seiler, and I.-O. Stamatescu, Phys. Rev. D **81**, 054508 (2010).
[22] G. Aarts, F. A. James, E. Seiler, and I.-O. Stamatescu, Phys. Lett. B **687**, 154 (2010).
[23] G. Aarts, F. A. James, E. Seiler, and I.-O. Stamatescu, Eur. Phys. J. C **71**, 1756 (2011).
[24] G. Aarts, F. A. James, J. M. Pawlowski, E. Seiler, D. Sexty, and I.-O. Stamatescu, J. High Energy Phys. 03 (2013) 073.
[25] L. L. Salcedo and E. Seiler, J. Phys. A **52**, 035201 (2019).
[26] Z. Cai, X. Dong, and Y. Kuang, SIAM J. Sci. Comput. **43**, A685 (2021).
[27] E. Seiler, D. Sexty, and I.-O. Stamatescu, Phys. Rev. D **109**, 014509 (2024).
[28] M. Scherzer, E. Seiler, D. Sexty, and I.-O. Stamatescu, Phys. Rev. D **99**, 014512 (2019).
[29] M. Scherzer, E. Seiler, D. Sexty, and I. O. Stamatescu, Phys. Rev. D **101**, 014501 (2020).
[30] E. Seiler, Phys. Rev. D **102**, 094507 (2020).
[31] K. Nagata, J. Nishimura, and S. Shimasaki, Phys. Rev. D **94**, 114515 (2016).
[32] K. Nagata, J. Nishimura, and S. Shimasaki, J. High Energy Phys. 05 (2018) 004.
[33] D. Alvestad, R. Larsen, and A. Rothkopf, J. High Energy Phys. 04 (2023) 057.
[34] K. Boguslavski, P. Hotzy, and D. I. Müller, J. High Energy Phys. 06 (2023) 011.
[35] N. M. Lampl and D. Sexty, arXiv:2309.06103.
[36] D. Alvestad, A. Rothkopf, and D. Sexty, Phys. Rev. D **109**, L031502 (2024).
[37] E. Seiler, D. Sexty, and I.-O. Stamatescu, Phys. Lett. B **723**, 213 (2013).
[38] G. Aarts, L. Bongiovanni, E. Seiler, D. Sexty, and I.-O. Stamatescu, Eur. Phys. J. A **49**, 89 (2013).
[39] K. Nagata, J. Nishimura, and S. Shimasaki, Prog. Theor. Exp. Phys. **2016**, 013B01 (2016).
[40] Z. Cai, Y. Di, and X. Dong, Commun. Comput. Phys. **27**, 1344 (2020).
[41] X. Dong, Z. Cai, and Y. Di, Phys. Rev. D **102**, 054518 (2020).
[42] G. Aarts, F. Attanasio, B. Jäger, and D. Sexty, J. High Energy Phys. 09 (2016) 087.
[43] D. Sexty, Phys. Lett. B **729**, 108 (2014).
[44] G. Aarts, E. Seiler, D. Sexty, and I.-O. Stamatescu, Phys. Rev. D **90**, 114505 (2014).
[45] Z. Fodor, S. D. Katz, D. Sexty, and C. Török, Phys. Rev. D **92**, 094516 (2015).
[46] K. Nagata, H. Matsufuru, J. Nishimura, and S. Shimasaki, Proc. Sci. LATTICE2016 (**2016**) 067 [arXiv:1611.08077].
[47] K. Nagata, J. Nishimura, and S. Shimasaki, Phys. Rev. D **98**, 114513 (2018).
[48] J. B. Kogut and D. K. Sinclair, Phys. Rev. D **100**, 054512 (2019).
[49] F. Attanasio, B. Jäger, and F. P. G. Ziegler, Eur. Phys. J. A **56**, 251 (2020).
[50] T. Yokota, Y. Ito, H. Matsufuru, Y. Namekawa, J. Nishimura, A. Tsuchiya, and S. Tsutsui, J. High Energy Phys. 06 (2023) 061.
[51] D. Sexty, Phys. Rev. D **100**, 074503 (2019).
[52] F. Attanasio, B. Jäger, and F. P. G. Ziegler, arXiv:2203.13144.
[53] F. Attanasio and B. Jäger, Eur. Phys. J. C **79**, 16 (2019).
[54] Z. Cai, Y. Kuang, and H. K. Tan, Phys. Rev. D **105**, 014508 (2022).
[55] P. H. Damgaard and H. Huffel, Phys. Rep. **152**, 227 (1987).
[56] M. W. Hansen, M. Mandl, E. Seiler, and D. Sexty, arXiv:2412.17137.
[57] G. Aarts and I.-O. Stamatescu, J. High Energy Phys. 09 (2008) 018.
[58] C. Gattringer and C. B. Lang, *Quantum Chromodynamics on the Lattice* (Springer, Berlin, 2010), Vol. 788, ISBN 978-3-642-01849-7, 978-3-642-01850-3.
[59] P. de Forcrand, Proc. Sci. LAT2009 (**2009**) 010 [arXiv:1005.0539].
[60] A. Hasenfratz and D. Toussaint, Nucl. Phys. **B371**, 539 (1992).
[61] M. Westh Hansen and D. Sexty, Proc. Sci. LATTICE2022 (**2023**) 163 [arXiv:2212.12029].
[62] M. W. Hansen and D. Sexty (to be published).
[63] T. D. Cohen, Phys. Rev. Lett. **91**, 222001 (2003).